Novel chemoresistive CH_4 sensor with 10 ppm sensitivity based on multiwalled carbon nanotubes functionalized with SnO_2 nanocrystals

Md Tanim Humayun, Ralu Divan, Yuzi Liu, Lara Gundel, Paul A. Solomon, and Igor Paprotny

Citation: Journal of Vacuum Science & Technology A: Vacuum, Surfaces, and Films **34**, 01A131 (2016);
View online: https://doi.org/10.1116/1.4936384
View Table of Contents: http://avs.scitation.org/toc/jva/34/1
Published by the American Vacuum Society

Novel chemoresistive CH_4 sensor with 10 ppm sensitivity based on multiwalled carbon nanotubes functionalized with SnO_2 nanocrystals

Md Tanim Humayun
Department of Electrical and Computer Engineering, University of Illinois, Chicago, Illinois 60607

Ralu Divan and Yuzi Liu
Center for Nanoscale Materials, Argonne National Laboratory, Lemont, Illinois 60439

Lara Gundel
Lawrence Berkeley National Laboratory, Berkeley, California 94720

Paul A. Solomon
U.S. Environmental Protection Agency, Las Vegas, Nevada 89199

Igor Paprotny[a)]
Department of Electrical and Computer Engineering, University of Illinois, Chicago, Illinois 60607

(Received 5 September 2015; accepted 11 November 2015; published 30 November 2015)

Chemoresistive sensors based on multiwalled carbon nanotubes (MWCNTs) functionalized with SnO_2 nanocrystals (NCs) have great potential for detecting trace gases at low concentrations (single ppm levels) at room temperature, because the SnO_2 nanocrystals act as active sites for the chemisorption of gas molecules, and carbon nanotubes (CNTs) act as an excellent current carrying platform, allowing the adsorption of gas on SnO_2 to modulate the resistance of the CNTs. However, uniform conjugation of SnO_2 NCs with MWCNTs is challenging. An effective atomic layer deposition based approach to functionalize the surface of MWCNTs with SnO_2 NCs, resulting in a novel CH_4 sensor with 10 ppm sensitivity, is presented in this paper. Scanning electron microscopy, transmission electron microscopy (TEM), energy dispersive x-ray spectroscopy, and Raman spectroscopy were implemented to study the morphology, elemental composition, and the crystal quality of SnO_2 functionalized MWCNTs. High resolution TEM images showed that the crystal quality of the functionalizing SnO_2 NCs was of high quality with clear lattice fringes and the dimension almost three times smaller than shown thus far in literature. A lift-off based photolithography technique comprising bilayer photoresists was optimized to fabricate SnO_2 functionalized MWCNTs-based chemoresistor sensor, which at room temperature can reliably sense below 10 ppm of CH_4 in air. Such low level gas sensitivity, with significant reversible relative resistance change, is believed to be the direct result of the successful functionalization of the MWCNT surface by SnO_2 NCs. [http://dx.doi.org/10.1116/1.4936384]

I. INTRODUCTION

Semiconductive SnO_2 is widely used in gas sensing metal oxide sensors.[1–5] However, the use of bare SnO_2 as a gas sensor is limited by the requirement for continuous heating to initiate the surface chemisorption of O_2; a prerequisite for the SnO_2 to react with the target gas species.[1–5] On the other hand, due to the excellent surface area to volume ratio and extraordinary electronic property arising from its one dimensional nanoscale cylindrical shape, carbon nanotubes (CNTs) show remarkable modulation of electrical properties, enabling the detection of low levels (about a ppm) of gaseous species at room temperature.[6–9] However, the surface of bare CNTs is nonreactive to many gas molecules, and in order to obtain a selective gas sensing, it is necessary to functionalize the surface of the CNTs, i.e., embedding it with active sites, by controlled deposition of functionalizing nanomaterials.[8–12] Thus, the nanoscale integration of SnO_2 and CNTs opens a unique path to building sensitive (less than ppm) and selective chemoresistor gas sensors that do not require external heat to operate, making this conjugate a more effective gas sensing element than either of its constituents.

In order to confirm a significant reversible relative resistance change at low level of the species of interest, it is necessary that the deposited SnO_2 nanocrystals (NCs) uniformly cover the surface of the multiwalled carbon nanotubes (MWCNTs). Most of the reported SnO_2-CNT nanohybrids are synthesized chemically, where the uniform coverage of the discrete NCs and their crystal quality cannot be precisely controlled.[13–15] In order to facilitate the control of the deposition of nanometers thick SnO_2 NCs on the surface of MWCNT, we developed site-specific atomic layer deposition (ALD) functionalization process. ALD is unique in that it is agnostic to complex substrates such as MWCNT mesh, and it enables precise, layer-by-layer control of the thickness and coverage of the deposited material.[16,17] In addition, to enhance the integration of the SnO_2 NCs with the MWCNTs, the surface of the MWCNTs was pretreated using a UV-O_3 based activation method.

CH_4 is one of the most important greenhouse gases with a 20-times higher impact on climate change than that of

[a)]Electronic mail: paprotny@uic.edu

CO_2.[18] Therefore, it is important to develop CH_4 sensors that have high sensitivity (i.e., strong relative change in sensing parameters), low detection limit (low ppm range), low cost, and are highly selective to CH_4. These sensors can be deployed across the natural gas and petroleum production, transmission, and distribution infrastructures to enable continuous monitoring of CH_4 emissions. Currently available methods for detecting CH_4 have several shortcomings, which prevent their wide-spread deployment. Besides high expense and low signal-to-noise ratio, existing infrared absorption-based CH_4 sensors suffer from nonselectivity to CH_4.[19] Widely used microfabricated metal oxide-based low cost CH_4 sensors require high power (more than 100s of mWs) for surface chemisorption of O_2.[1–3,5] Functionalized CNT-based CH_4 sensors, which can detect CH_4 at room temperature, have also been reported;[8,20,21] however, they show a poor irreversible relative resistance change at low ppm levels of CH_4,[8,20,21] which might be the result of: (1) an ineffective functionalization method, i.e., nonuniform coverage of the functionalizing nanoparticles (NPs) on the CNT surface, (2) weaker bonding between the functionalizing material and CNT surface resulting from lack of surface activation by pretreatment methods, (3) poor crystal quality of the functionalizing NPs, and (4) high Schottky barrier at the junction of the CNT and the functionalizing NPs. In addition, the reported functionalization materials for the CNT-based CH_4 chemoresistor sensors, such as Pd, are expensive.[9]

Our highly sensitive SnO_2 NC-functionalized MWCNTs CH_4 sensor overcomes the aforementioned limitations due to: (1) the ALD technique we used ensures uniform coverage of SnO_2 NCs on the MWCNT surface,[22,23] (2) the UV-O_3 based surface pretreatment creates nucleation sites on the MWCNTs ensuring strong bonding between SnO_2 and MWCNT, as well as high crystal quality of the deposited SnO_2 NCs,[24] (3) the work function between SnO_2 and MWCNTs is more similar hence low Schottky barrier at the junction,[9] and (4) SnO_2 is also less expensive[9] than other functionalization materials used in reported CNT-based CH_4 chemoresistor sensors.

II. FABRICATION

A 1 μm thick SiO_2 layer was grown on Si(100) wafers using wet oxidation at a temperature of 1100 °C for 3 h. Following the growth of the oxide layer, a set of interdigitated gold (Cr/Au) electrodes were fabricated on the SiO_2 coated Si wafer implementing a lift-off based photolithography technique. Gaps between the interdigitated electrodes ranged from 5 to 10 μm.

A batch of 98% pure MWCNTs with 12 nm average diameter, 10 μm average lengths, and a specific surface area of 220 m^2/g was purchased from Sigma Aldrich. An ultrasonicated solution of 1 mg/50 ml of MWCNTs/ethanol was used to produce a well dispersed MWCNT mesh. Using a microsyringe, a 50 μl aliquot was deposited on a 1 mm^2 active area of the fabricated metal electrodes, which was followed by baking at 75 °C to remove the solvent and to improve adhesion.

The deposited MWCNTs were treated with UV-O_3 inside a UV-O_3 chamber (Nanonex Ultra-100), for durations varying from 15 to 20 min. ALD was used to integrate SnO_2 NCs with surface pretreated MWCNTs. The growth was done using an Ultratech Savannah S200. The tetrakis(dimethylamino) tin(IV) was heated to 55 °C and delivered under its own vapor pressure in a 1 s pulse, followed by a 15 s purge, a 0.1 s water dose, and another 15 s purge. This process was repeated for 175 cycles at a growth temperature of 175 °C.[22] ALD resulted in a deposition of SnO_2 NCs with an average diameter of 3.36 nm and confirmed by transmission electron microscope (TEM).

The electrical conductivity of the fabricated electrodes, the CNT-deposited resistive network, and ALD-functionalized MWCNTs devices was measured using a digital multimeter (Fluke 115). Parasitic and contact resistance was on the order of single ohms and considered insignificant compared to the resistance of the chemoresistor (1–100 kΩ).

The MWCNTs functionalized with the SnO_2 NCs were characterized using several approaches. Scanning electron microscope (SEM; Raith 150) was used to characterize their morphology. Energy dispersive x-ray spectroscopy (EDX; Nova 600 Nanolab Dualbeam SEM/FIB) was applied to characterize the elemental composition of SnO_2-MWCNT samples. A micro-Raman system (Renishaw Invia) was used to perform green laser (wavelength of 514 nm) Raman spectroscopy on the SnO_2 NC functionalized MWCNT samples at room temperature. A JEOL 2100F TEM operated at 200 kV was used to characterize atomic scale morphology and crystal quality of the SnO_2 NCs deposited on MWCNT surfaces.

III. EXPERIMENTAL SETUP

SnO_2-MWCNT sensors were evaluated in a test chamber connected with inlets and outlets for gases and an inlet for the electrical feedthroughs. The residence time of the chamber was 4.5 min at a flow rate of 0.94 l/min. The relative humidity (RH) and temperature inside the test chamber were continuously monitored and recorded by a commercial datalogger (HOBO U-10 series). The real-time electrical signals generated from the sensors were recorded by a computer employing a custom interface circuit and an analog-to-digital converter. A mixture of 10 ppm methane in dry air (Praxair, Inc.) was introduced to the chamber at a constant flow rate (0.94 l/min) and monitored by a rotameter for 30 min. The relative humidity inside the test chamber was kept constant, confirmed by a data-logging humidity sensor (HOBO U-10 series). Dry N_2 was used to purge CH_4 from the chamber and to return the devices back to their baseline resistance after each cycle of CH_4 exposure.

To study the interference of water vapor on sensor performance, the relative resistance change of the sensor was monitored while the RH inside the sealed test chamber was maintained above 80% for almost 24 h. After this period, the RH was reduced back approximately to 10% by flowing dry air through the test chamber.

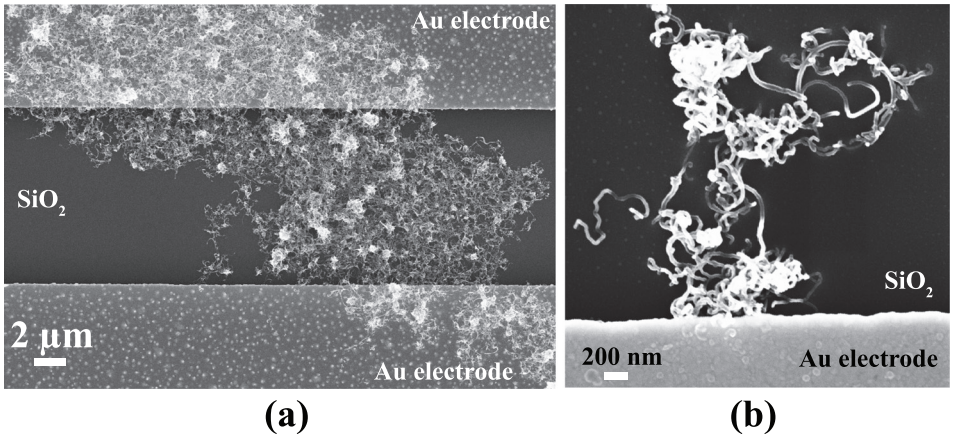

FIG. 1. (a) SnO_2 NCs functionalized MWCNTs mesh trapped between two fingers of an interdigitated Au electrode network. (b) Higher magnification SEM image focusing MWCNTS mesh. Brighter surface of the MWCNTs is a result of SnO_2 NCs functionalization.

To understand the response of the sensor to CH_4 at relatively higher RH, 10 ppm of CH_4 was allowed to flow through a water bubbler at a constant flow rate (0.94 l/min) maintaining RH inside the test chamber equal to about 70%. After the CH_4 cycle, N_2 was allowed to flow through the water bubbler at the same flow rate to recover the sensor's original response.

IV. RESULTS

In order for the MWCNT network to function as a chemoresistor, the ALD-deposited SnO_2 cannot create a direct conductive pathway between the electrodes outside the MWCNT mesh, i.e., the sensor electrodes are only connected via the MWCNTs and not the deposited SnO_2. This was confirmed with electrical testing; depending on the structure of the interdigitated metal electrodes and the density of the deposited MWCNT in the ethanol solution, the resistance of the MWCNT-connected electrodes in our sensors varied between 1 and 100 kΩ, while the resistance outside of the MWCNT mesh was found to be infinite.

SEM images confirmed that the functionalized MWCNTs were in proper contact with the interdigitated Au metal pads (Fig. 1). SEM and EDX results show that the SnO_2 NCs were present on the MWCNTs surface, confirmed by the stronger Sn signal as indicated by the brighter regions in Fig. 2 (points 3, 4, and 5).

The TEM micrograph shows discrete SnO_2 NCs uniformly covering the surface of the pretreated MWCNT surface [Fig. 3(a)]. The inset shows the size distribution of the ALD deposited SnO_2 NCs on the MWCNT surface. The mean diameter of the "spherical" SnO_2 NCs was found to be 3.36 nm with a standard deviation of 0.76 nm. Average SnO_2 NC size was smaller in comparison with existing works.[8] The high resolution TEM (HRTEM) image in Fig. 3(b) illustrates the rutile structure of the SnO_2 NC and its good crystalline quality. The interplanar spacing of 3.3 and 2.6 Å correspond to lattice spacing of rutile SnO_2 from ⟨110⟩, ⟨101⟩ reflections, respectively.[9]

Raman spectra, illustrated in Fig. 4, reveal that after the surface pretreatment and ALD functionalization, the D, G, and G' peaks of the MWCNT are preserved, while additional Raman peak originating from the SnO_2 NCs appeared.

The D band frequency position was 1349.56 and 1350.7 cm^{-1}, respectively, for pristine and SnO_2 functionalized MWCNT. The G band frequency position was 1573.74 and 1577.9 cm^{-1}, respectively, for pristine and SnO_2 functionalized MWCNT. Although the D band frequency was almost same for both type of samples, the G band frequency showed upward shift in case of SnO_2 functionalized

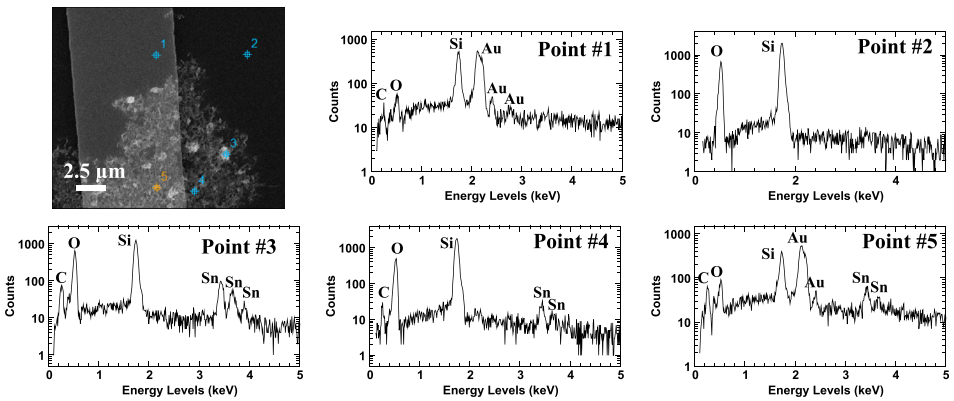

FIG. 2. (Color online) EDX plots obtained from various points on a SnO_2 NCs functionalized MWCNTs device. Signal of C, Sn, and O originated from the points located on functionalized MWCNT surface. Strength of Sn signal varied according to the brightness of points on the SEM micrograph.

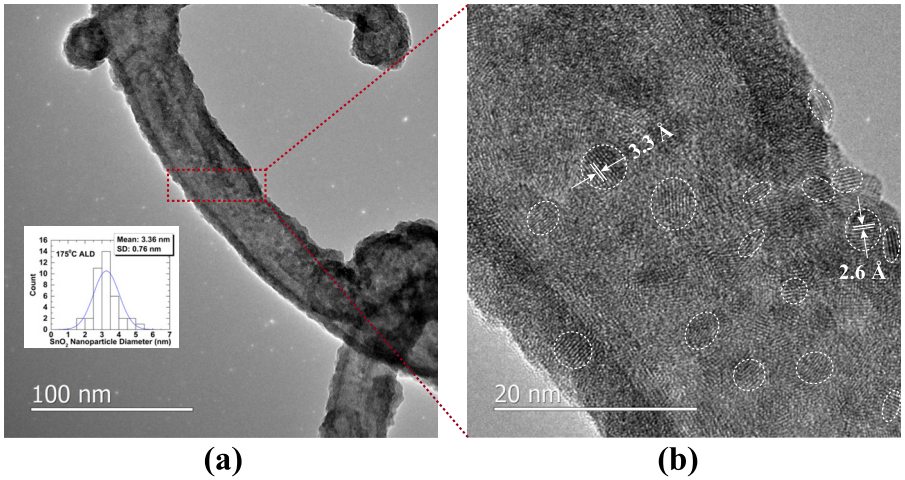

FIG. 3. (Color online) (a) TEM image of a single MWCNT functionalized by SnO_2 nanocrystals. Inset shows the statistical size distribution of functionalizing SnO_2 NCs with a mean diameter of 3.36 nm. (b) HRTEM image showing the lattice fringes originated from SnO_2 NCs. Boundaries of the SnO_2 NCs are marked with white dashed line in order to guide reader's view. Interplanar spacing of 3.3 and 2.6 Å correspond to lattice spacing of rutile SnO_2 from ⟨110⟩, ⟨101⟩ reflections, respectively.

MWCNT. The *G*-band has been attributed to the tangential mode (TM) C–C stretching vibrations.[25] This upward shift of *G* band frequency (or "stiffening" of the TM) was interpreted as electron transfer from carbon atoms to acceptor atoms during surface treatment of CNTs.[25] The I_D/I_G ratio was found to be 0.81 and 1.02, respectively, for pristine and SnO_2 loaded MWCNT [Figs. 4(a) and 4(b)]. The *D* peak generally represents the defect or sp^3 carbon on the curved graphitic sheet. The ratio I_D/I_G, where *I* represents the intensity of the Lorentzian function of the *D* and *G* peak, allows for an estimate of the presence of a defect on the MWCNT surface.[25–27] The increase in the intensity of the *D* peak with respect to the *G* peak may be caused by the presence of reactive sites on the surface of the MWNTs.[25,27] The tube sidewalls are strongly disrupted as a result of the prolonged interaction with reactive O_3 during UVO_3 treatment.[27] In our case, UVO_3-based surface treatment may give rise to these reactive sites, which help nucleating the SnO_2 nanoparticles enhancing their uniform distribution on the MWCNT surface.

The characteristic Raman peak with a frequency shift of 628.38 cm^{-1} corresponds to A_{1g} mode of SnO_2.[28] The nondegenerate mode A_{1g} vibrates in the plane perpendicular to the c axis.[29] This is a normal vibrational mode of bulk SnO_2 but gets modified in the case of SnO_2 nanoparticles.[29]

The polynomial fitting for the phonon dispersion curve of the A_{1g} mode has been reported as[29]

$$\omega(q) = A + B_1(q\pi) + B_2(q\pi)^2 + B_3(q\pi)^3 + B_4(q\pi)^4 + B_5(q\pi)^5,$$

with, $A = 638.22\ cm^{-1}$, $B_1 = -2.81\ cm^{-1}$, $B_2 = 6.52\ cm^{-2}$, $B_3 = -7.25\ cm^{-3}$, $B_4 = 0.27\ cm^{-4}$, and $B_5 = 0.21\ cm^{-5}$.

In infinite crystals, phonons only near the center of the Brillouin zone, with $q = 0$, contribute to the Raman scattering of the incident light. On the other hand, in nanodimensional crystal, phonons with nonzero q also contribute to the Raman scattering of the incident light. Hence, $\omega(q)$ starts shifting from $A = 638.22\ cm^{-1}$. Thus, as the size of the SnO_2 reduces and enters nanoscale regime, A_{1g} mode shifts to lower wave number.[29] In our SnO_2 nanocrystals, the observed A_{1g} Raman mode at 628.38 cm^{-1} is almost 10 cm^{-1} lower in comparison to the A_{1g} peak of 638.22 cm^{-1} for bulk SnO_2.[28,29] Hence, the Raman behavior of our SnO_2 NCs is consistent with reported studies.[29]

When exposing the SnO_2-functionalized MWCNT chemoresistor sensor to 10 ppm of CH_4 in dry air, we observed a reproducible resistance change. Methane exposure experiments were carried out at constant RH (1.5%). Figure 5 shows the positive relative resistance change $(\Delta R/R = (R_{methane} - R_{air})/R_{air})$ of a SnO_2-MWCNT sensor

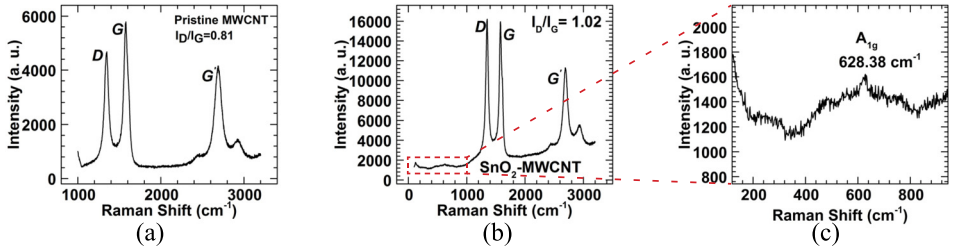

FIG. 4. (Color online) (a) Room temperature Raman spectrum obtained from (a) pristine MWCNT, and (b) SnO_2 NCs functionalized MWCNTs while excited by a green laser with 514 nm of wavelength. (c) Magnified plot emphasizes on the A_{1g} peak of SnO_2.

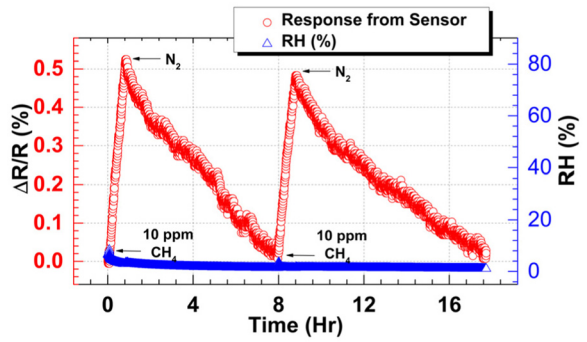

FIG. 5. (Color online) Relative resistance change of the SnO_2-MWCNT chemoresistor sensor while exposed to 10 ppm of CH_4 in dry air and N_2 in an iterative fashion. The circle symbol plot represents relative resistance change ($\Delta R/R = (R_{methane} - R_{air})/R_{air}$) of the chemoresistor sensor (left hand, y-axis) while the triangle symbol plot represents the RH inside the test chamber recorded by a commercial RH data logger, HOBO (right hand, y-axis).

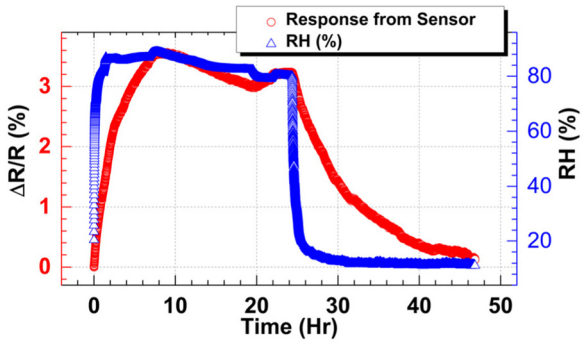

FIG. 6. (Color online) Response from the SnO_2-MWCNT chemoresistor sensor to RH variation inside the test chamber. The circle symbol plot represents relative resistance change ($\Delta R/R = (R_{water} - R_{air})/R_{air}$) of the chemoresistor sensor (left hand, y-axis) while the triangle symbol plot represents the RH inside the test chamber recorded by a commercial RH data logger, HOBO (right hand, y-axis).

(20 min UV-O_3 treatment and SnO_2 ALD at 175 °C) each time it was exposed to 10 ppm of CH_4 in dry air at a constant flow rate (0.94 l/min). The resistance of the sensor repeatedly returned back to its original level when the test chamber was purged with dry N_2 at the end of each CH_4 exposure cycle. No response to CH_4 was observed for sensors fabricated with nonfunctionalized MWCNTs.

MWCNTs act like a rolled up graphene sheet with an electrical property similar to crystalline graphite, with overlapping conduction and valence bands.[30] Hence, the MWCNT shows a metallic type electrical property. However, the presence of p-type semiconductive MWCNTs has also been reported.[9,30] Lu *et al.*[9] has shown that when SnO_2-MWCNT comes in contact with oxidizing gas such as NO_2, the conductance of the p-type MWCNT increases.[9] As electrons are accepted by the oxidizing NO_2 molecules, the depletion region at the junction of the n-type SnO_2 and p-type MWCNT increases. The position of the Fermi level (E_F) is also altered at the p-type MWCNT, E_F shifts closer to the valence band. As a result, the electrical conductance of the p-type MWCNT increases. Accordingly, if the SnO_2-MWCNT hybrid structure interacts with reducing CH_4, the electrical conductance of the p-type MWCNT is supposed to decrease. The results presented here corroborate this hypothesis and describe the relative change in resistance as follows:

$$\Delta R/R = (R_{\text{methane}} - R_{\text{air}})/R_{\text{air}}.$$

The RH interference test indicated that the sensor resistance varied with RH inside the test chamber; suggesting electron transport between the H_2O molecules and the SnO_2-MWCNT chemoresistor sensors, i.e., strong RH sensitivity of the sensors (Fig. 6).

Because the sensors respond strongly to a change in RH, caution was taken during the CH_4 tests to keep the RH inside the test chamber constant (Fig. 5).

When exposing the SnO_2-functionalized MWCNT chemoresistor sensor to 10 ppm of CH_4 in dry air at the higher RH (approximately 70%), we observed a similar monotonic resistance increment (Fig. 7b) compared to the low RH tests [Fig. 7(a)] where RH was held constant at a few percent. The sensor also equilibrated to its original response in a similar fashion when the chamber was purged with N_2. The sensitivity to CH_4 and signal-to-noise ratio reduced in comparison to those at lower RH, which we believe was a result of adsorbed H_2O molecules on the SnO_2-MWCNT sensor. Although the sensor showed reduced response it was still capable of detecting 10 ppm CH_4 at 70% RH. A noticeable behavior on the sensor performance is the shorter recovery time of the sensor at lower RH shown in Fig. 7(a) in comparison to the result shown in Fig. 5. We observed an improvement of the sensor performance with respect to recovery time after almost 2.5 months of extensive use. Similar effects have been reported in the literature. For example, Sayago *et al.*[31] reported that their CNT-based H_2 sensors showed significant improvement with regard to response and recovery times as the sensors aged. The improvement was postulated to be an effect of introduction of carboxylic functionalities due to oxygen exposure. Further research to study the aging related changes in the chemical composition of the SnO_2-MWCNT nanohybrids is necessary and has been reserved for future work.

CNT arrays, functionalized with various metal nanoparticles, can potentially distinguish gas phase species in a multicomponent environment.[32,33] To create selectively functionalized CNT arrays, electroplating and sputtering-based functionalization techniques have been pursued[32,33] Chemical analysis of a multicomponent gas mixture has been performed based on the response from various components of the arrays. Our recent results showed that MWCNT meshes—functionalized with various metal oxide nanoparticles, such as ZnO and SnO_2—have different degrees of response to RH. As implemented by other groups for increasing selectivity to target gases, we plan to fabricate a network of MWCNTs selectively functionalized with various metal oxide nanoparticles. By deconvoluting the constructive/destructive interference in the presence of various RH levels, the RH contribution can be effectively determined and removed from the CH_4 response.

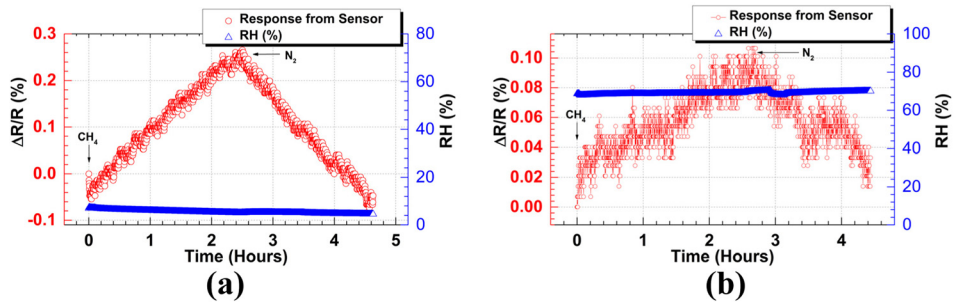

FIG. 7. (Color online) Relative resistance change of the SnO_2-MWCNT chemoresistor sensor while exposed to 10 ppm of CH_4 in dry air at (a) a lower RH (approximately 5%), and (b) a higher RH (approximately 70%) and was recovered by N_2. The circle symbol plot represents relative resistance change ($\Delta R/R = (R_{methane} - R_{air})/R_{air}$) of the chemoresistor sensor (left hand, y-axis) while the triangle symbol plot represents the RH inside the test chamber recorded by a commercial RH data logger, HOBO (right hand, y-axis).

Here, we summarized the results of state-of-the-art room temperature CH_4 sensors reported by various groups and compared the performance of our sensor with those. Previously, an electron beam evaporation-based Pd loaded SWCNT (not preactivated) CH_4 sensor has been reported.[8] The sensitivity ($\Delta I/I$) was approximately 0.02 while the sensors were exposed to 15 ppm CH_4 in air for 10 min at a temperature of 40 °C. At 15 ppm CH_4, the response and recovery times were 10 and 30 min (using UV), respectively. The authors also reported a sensitivity ($\Delta I/I$) of approximately 0.01–10 ppm of CH_4 at room temperature. Replicate data and RH control were not presented for the room temperature test. Li *et al.*[21] reported a CH_4 chemoresistive sensor containing Pd NP deposited on 1,6-hexanediamine grafted MWCNTs. The sensitivity ($\Delta R/R$) of the sensor was 0.03 at 3 vol. % (30 000 ppm) CH_4 in air at room temperature. The response and recovery times were 10 and 30 s, respectively. RH control was not reported. Yang and Sacher[34] reported a composite of Pd and MWCNTs prepared by reducing their aqueous mixtures with $NaBH_4$. The uniformity of the functionalized NPs was poor. The sensors were tested with 2 vol. % (20 000 ppm) CH_4 in N_2 showing a room temperature sensitivity ($\Delta R/R$ in percent) of 4.5%. The response and recovery time was 310 and 176 s, respectively. Biaggi-Labiosa *et al.*[35] reported a mixture of porous SnO_2 nanorods and MWCNTs. Sensors exhibited response and recovery times in tens of minutes while being tested with 2500 ppm CH_4 at room temperature.

Compared to these related previous studies, the principal limitations of our sensor are: (1) long response and recovery times and (2) a low relative resistance change. However, the principal advantages over these related studies are: (1) response at significantly lower concentrations (10 ppm) of CH_4 in a reproducible manner at room temperature (20 °C), and (2) more reliable and reproducible tests as the RH was carefully tracked during our testing, in contrast with the previously published results. It should be pointed out that although the saturation time in our sensor was longer, it is still at the same order of magnitude as other published results,[8] despite being at lower concentration and not heated (at room temperature).

In addition, the response transients in Figs. 5 and 7 are not saturated. However, we have conducted preliminary tests indicating that the sensor takes approximately 3 h to reach saturation. The slow diffusion and weaker absorption of the gas molecules on the surface of the chemoresistive sensor likely are the principal cause for the longer response time.[35–38] For our sensor, the long response time may also be a result of slow diffusion and weak absorption of the gas molecules onto the functionalized MWCNT surface. This hypothesis can be further investigated in two ways: (1) by reducing the number of ALD cycles when functionalizing the MWCNTs with SnO_2, which should reduce the thickness of the SnO_2 NPs and improve their discreteness on the MWCNT surface, and (2) in a related work, we observed that the mean size of functionalizing ZnO NPs on MWCNTs reduces as the ALD temperature increases.[39] The crystalline quality of the functionalizing ZnO NPs also improves with higher temperature ALD. In future, we plan to increase the ALD temperature for SnO_2 functionalization in order to reduce the size of the NPs and to improve crystalline quality. Functionalizing NPs with reduced dimension and high crystal quality should improve the gas molecule diffusion to, and absorption on, the sensor surface. These effects will be investigated in the future work.

V. CONCLUSION

The resultant SnO_2 NC functionalized MWCNT chemoresistor CH_4 sensors exhibited reproducible relative resistance change to 10 ppm level of CH_4 in dry air at room temperature, which, we believe, is a result of: (1) uniform distribution of discrete SnO_2 NCs on MWCNTs surface, (2) strong sensitivity of SnO_2 NCs to CH_4 molecules, and (3) low Schottky barrier at the SnO_2-MWCNT junction. A uniform controlled deposition of discrete SnO_2 NCs on the MWCNT surface was achieved through an optimized ALD process. Various characterization results show that SnO_2 NCs on MWCNT surface have smaller dimension and better crystal quality in comparison with other existing results from the literature. Future work will focus on different pretreatment methods of MWCNT surfaces and their effect on the sensor performance. Ongoing work in our laboratory among others continues to investigate the effect of other possible interfering gases. The presented sensor, once fully

characterized, is envisioned to enable low cost distributed leak detection for the natural gas infrastructure.

ACKNOWLEDGMENTS

The authors would like to thank Alex B. Martinson for SnO_2 deposition by ALD and Daniel Rosenmann for metal deposition. Use of the Center for Nanoscale Materials, an Office of Science user facility, was supported by the U.S. Department of Energy, Office of Science, Office of Basic Energy Sciences, under Contract No. DE-AC02-06CH11357. The project is also in part funded by a grant from Aclima Inc., award No. 2015-07496. The U.S. Environmental Protection Agency, through its Office of Research and Development, collaborated in the research described here. It has been subjected to Agency review and approved for publication.

[1]P. Fau, M. Sauvan, S. Trautweiler, C. Nayral, L. Erades, A. Maisonnat, and B. Chaudret, Sens. Actuator B **78**, 83 (2001).
[2]D.-D. Lee, W.-Y. Chung, and B.-K. Sohn, Sens. Actuator B **13**, 252 (1993).
[3]B. K. Min and S. D. Choi, Sens. Actuator B **98**, 239 (2004).
[4]M. Nitta and M. Haradome, J. Electron. Mater. **8**, 571 (1979).
[5]F. Quaranta, R. Rella, P. Siciliano, S. Capone, M. Epifani, L. Vasanelli, A. Licciulli, and A. Zocco, Sens. Actuator B **58**, 350 (1999).
[6]T. Zhang, S. Mubeen, N. V. Myung, and M. A. Deshusses, Nanotechnology **19**, 332001 (2008).
[7]M. S. Dresselhaus, G. Dresselhaus, and R. Saito, Carbon **33**, 883 (1995).
[8]Y. Lu, J. Li, J. Han, H.-T. Ng, C. Binder, C. Partridge, and M. Meyyappan, Chem. Phys. Lett. **391**, 344 (2004).
[9]G. Lu, L. E. Ocola, and J. Chen, Adv. Mater. **21**, 2487 (2009).
[10]J. Kong, M. G. Chapline, and H. Dai, Adv. Mater. **13**, 1384 (2001).
[11]C. Staii, A. T. Johnson, M. Chen, and A. Gelperin, Nano Lett. **5**, 1774 (2005).
[12]P. Qi, O. Vermesh, M. Grecu, A. Javey, Q. Wang, H. Dai, S. Peng, and K. Cho, Nano Lett. **3**, 347 (2003).
[13]Y.-L. Liu, H.-F. Yang, Y. Yang, Z.-M. Liu, G.-L. Shen, and R.-Q. Yu, Thin solid films **497**, 355 (2006).
[14]J. G. Zhou, H. T. Fang, J. M. Maley, J. Y. P. Ko, M. Murphy, Y. Chu, R. Sammynaiken, and T. K. Sham, J. Phys. Chem. C **113**, 6114 (2009).
[15]H.-X. Zhang, C. Feng, Y.-C. Zhai, K.-L. Jiang, Q.-Q. Li, and S.-S. Fan, Adv. Mater. **21**, 2299 (2009).
[16]M.-G. Willinger, G. Neri, E. Rauwel, A. Bonavita, G. Micali, and N. Pinna, Nano Lett. **8**, 4201 (2008).
[17]S. Boukhalfa, K. Evanoff, and G. Yushin, Energy Environ. Sci. **5**, 6872 (2012).
[18]"Overview of greenhouse gases." http://epa.gov/climatechange/ghgemissions/gases/ch4.html, accessed 2 September 2015.
[19]C. Massie, G. Stewart, G. McGregor, and J. R. Gilchrist, Sens. Actuator B **113**, 830 (2006).
[20]Y. Li, H. Wang, Y. Chen, and M. Yang, Sens. Actuator B **132**, 155 (2008).
[21]Z. Li, J. Li, X. Wu, S. Shuang, C. Dong, and M. M. F. Choi, Sens. Actuator B **139**, 453 (2009).
[22]J. W. Elam, D. A. Baker, A. B. F. Martinson, M. J. Pellin, and J. T. Hupp J. Phys. Chem. C **112**, 1938 (2008).
[23]K. E. Aasmundtveit, B. Q. Ta, A. V. Ngo, O. Nilsen, and N. Hoivik, *2014 IEEE 14th International Conference on Nanotechnology (IEEE-NANO)* (IEEE, 2014).
[24]E. Najafi, J.-Y. Kim, S.-H. Han, and K. Shin, Colloid Surf. A **284**, 373 (2006).
[25]Z. N. Utegulov, D. B. Mast, P. He, D. Shi, and R. F. Gilland J. Appl. Phys. **97**, 104324 (2005).
[26]E. F. Antunes, A. O. Lobo, E. J. Corat, and V. J. Trava-Airoldi, Carbon **45**, 913 (2007).
[27]C. Chen, B. Liang, A. Ogino, X. Wang, and M. Nagatsu, J. Phys. Chem. C **113**, 7659 (2009).
[28]K. Mcguire, Z. W. Pan, Z. L. Wang, D. Milkie, J. Menendez, and A. M. Rao, J. Nanosci. Nanotechnol. **2**, 499 (2002).
[29]A. Dieguez, A. Romano-Rodriguez, A. Vila, and J. R. Morante, J. Appl. Phys. **90**, 1550 (2001).
[30]O. K. Varghese, P. D. Kichambre, D. Gong, K. G. Ong, E. C. Dickey, and C. A. Grimes, Sens. Actuator B **81**, 32 (2001).
[31]I. Sayago *et al.*, Sens. Actuator B **122**, 75 (2007).
[32]M. Penza, R. Rossi, M. Alvisi, and E. Serra, Nanotechnology **21**, 105501 (2010).
[33]A. Star, V. Joshi, S. Skarupo, D. Thomas, and J.-C. P. Gabriel, J. Phys. Chem. B **110**, 21014 (2006).
[34]D.-Q. Yang and E. Sacher, J. Phys. Chem. C **112**, 4075 (2008).
[35]A. Biaggi-Labiosa, F. Solá, M. Lebrón-Colón, L. J. Evans, J. C. Xu, G. W. Hunter, G. M. Berger, and J. M. González, Nanotechnology **23**, 455501 (2012).
[36]S. T. Shishiyanu, T. S. Shishiyanu, and O. I. Lupan, Sens. Actuator B **107**, 379 (2005).
[37]L. V. Thong, N. D. Hoa, D. T. Thanh Le, D. T. Viet, P. D. Tam, Anh-Tuan Le, and V. H. Nguyen, Sens. Actuator B **146**, 361 (2010).
[38]S. Roy and S. Basu, Bull. Mater. Sci. **25**, 513 (2002).
[39]M. T. Humayun, R. Divan, L. Stan, A. Gupta, D. Rosenmann, L. Gundel, P. A. Solomon, and I. Paprotny, J. Vac. Sci. Technol. B **33**, 06FF01 (2015).